Catalysis Letters Vol. 106, Nos. 1–2, January 2006 (© 2006)
DOI: 10.1007/s10562-005-9186-3

Synthesis of novel TiO_2 by mechanical alloying and heat treatment-derived nanocomposite of TiO_2 and $NiTiO_3$

Dong Hyun Kim[a,*], Ha Sung Park[a], Sun-Jae Kim[b], and Kyung Sub Lee[a]

[a]*Division of Materials Science & Engineering, Hanyang University, Seoul, 133-171, Korea*
[b]*Department of Nano Sci. & Tech/SAINT, Sejong University, Seoul, 143-747, Korea*

Received 7 July 2005; accepted 29 September 2005

A novel nanocomposite titanium dioxide powders were synthesized by mechanical alloying and heat treatment. The absorption threshold of the nanocomposite TiO_2 moved to a longer wavelength and the photoreactivity was dramatically enhanced. Also the new absorption was believed to be induced by the trapping band gap between the valence and conduction bands of nanocomposite TiO_2.

KEY WORDS: titanium dioxide; photocatalyst; mechanical alloying; titanate; nickel.

1. Introduction

Titanium dioxide is widely used as a photocatalyst, because of its chemical stability, low cost and harmless nature in the human body. However, TiO_2 becomes active only under ultraviolet light which has an energy greater than the band gap of TiO_2 (~3.0 eV). Overcoming the lack of a reaction in the visible light region is the focus of current TiO_2 research. Therefore, many studies have sought to improve the photocatalytic properties of TiO_2 by doping with cation [1] or anion metals [2] and oxides [3]. However, the photocatalystic properties of the cation-doped TiO_2 decreased even in the UV region. This is because the doped materials have an increase in the carrier-recombination centers and are unstable at high temperature [4]. Also, the absorption spectra of anion-doped TiO_2 in the visible light region are in the comparatively small range of about 400 nm [5].

Recently, Lin *et al.* [6] reported that nickel titanate can decompose the organic compounds by a photocatalystic reaction. Nickel titanate ($NiTiO_3$) has attracted a great deal of interest for use in chemical and electric materials due to its weak magnetism and semiconductivity. Conventionally, preparation of $NiTiO_3$ requires sintering of NiO and TiO_2 at high temperature. The sintering process causes the grain growth which prohibits the production of nanoscaled $NiTiO_3$ powder [7].

In our previous study, nanocrystalline Ni-doped rutile TiO_2 synthesized by mechanical alloying (MA) and HPPLT (Homogeneous Precipitation Process at Low Temperatures) exhibited an absorption threshold in the range of 480–500 nm [8]. However, this is a very small region in the visible light spectrum. In the current study, a novel nanocomposite titanium dioxide (Ni-doped $TiO_2 + NiTiO_3$ by heat treatment) was synthesized by MA and heat treatment. The photocatalytic behaviors of the powders were characterized by measuring the visible light reaction capacity. The detailed microstructural characteristics of the novel nanocomposite TiO_2 and the effect of $NiTiO_3$ formation was also investigated.

2. Experimental

Novel nanocomposite TiO_2 powders were prepared by MA and heat treatment. MA is a very effective process for refining grain size down to the nano-sized range and has the ability to alloy immiscible elements. In order to get a better doping effect, meta-stable rutile powder was selected as the starting powder for MA, instead of a stable TiO_2 phase. To obtain the meta-stable powder, a $TiO(OH)_2$ precipitate slurry was first prepared from $TiOCl_2$ using the HPPLT process [9]. Then, the solution was filtered using distilled water. The detailed HPPLT process has been reported elsewhere [9,10]. The filtered precipitates were dried at 60 °C for 12 h to obtain the dried TiO_2 powder. The dried powder was mechanically alloyed for 14 h by a planetary ball mill (Fritz mill, P-5) with nickel powders (KOJUNDO Chem. CO., LTD, 99.9%). The content of the Ni was 8 wt%. The ball-milling speed was 150 rpm and the ball to powder weight ratio was 15:1. In order to control of the impurity effect, the ZrO_2 ball (1 mm diameter) and bowl were used in the ball milling. After milling, the powders were treated at 1000 °C for 4 h in order to obtain the composite powders.

The structural properties of the alloying process and nanocrystallization process including grain size

* To whom correspondence should be addressed.
E-mail: dhk@ihanyang.ac.kr

determination were characterized by XRD ($Cu_{K\alpha}$, Rigaku D-MAX 3000) and by transmission electron microscopy (TEM, 200 KV, JEM 2000). The characteristics of the visible light reaction were investigated by UV/VIS-DRS (diffuse reflectance spectroscopy, Perkin-Elmer) and photoluminescence (PC-1 Photon counting fluorescence spectrometer). In addition, the synthesized powder was compared to commercial $NiTiO_3$ (KOJ-UNDO Chem. CO., LTD, 99.9%) powder and the simple mixture powder of our synthesizing rutile TiO_2 and $NiTiO_3$ (5 wt%), synthesizing rutile TiO_2 and P-25. Photocatalytic reaction of the powders was estimated by measuring the decomposition rates of 4-chlorophenol (0.1 mmol) in aqueous solution (500 ml) containing 0.1 g of various powders. As the light source a fluorescence lamp (380–800 nm) for visible light and 80 W pressure mercury arc lamp for ultra violet light were used, which was placed at about 20 cm from the quartz beaker. The solution was continuously stirred. During irradiation, the solution was took out at 5, 20, 35 min, each 50 ml. After the photolysis, the remaining carbon concentrations in the aqueous solutions were detected by a total organic carbon analyzer (SHIMADZU 4000 autosampler).

3. Results and discussion

Figure 1 shows the X-ray diffraction pattern for P-25, rutile, $NiTiO_3$, the alloyed powder (Ni-doped TiO_2), the alloyed powder after heat treatment and simple mixture of rutile and $NiTiO_3$ powder, respectively. It can be seen that alloyed powder and rutile powder consisted of only a rutile phase, and the main peak of alloyed powder shifted from the original rutile's main peak. This indicates that there was grain refinement of the average grain size and an increase in the internal strain by a mechanical deformation during ball milling [11]. Also, P-25 powder is a mixture of rutile and anatase phases. However, after heat treatment, the alloyed powder formed composite of the $NiTiO_3$ and rutile phase. The weight percent of $NiTiO_3$ in alloyed powder was calculated to be 5 wt% with the following equation [12]:

$$\text{Content of } NiTio_3 = \left\{ \frac{I_{NiTiO_3}}{I_{NiTiO} + 1.265 I_R} \right\} \times 100$$

where I_{NiTiO3} and I_R are peak intensities of $NiTiO_3$ and rutile, obtained from X-ray diffraction patterns. It is thought that heat treatment caused a portion of the Ni-doped TiO_2 to form a stable $NiTiO_3$ phase. However, the peak of the alloyed powder after heat treatment remained broadening and their intensities decreased with heating. It means that the grain growth did not occur through heat treatment because of drag effect [13]. Owing to $NiTiO_3$ segregation in Ni-doped TiO_2 matrix, grain boundary mobility was controlled by the lattice diffusion of the $NiTiO_3$ [14,15].On the other hand, simple mixture powders showed the coexistence of $NiTiO_3$ and rutile TiO_2 phase. Applying the Debye–Scherrer formular [11] and the full width at half maximum (FWHM) to the (110) reflection, typical values of crystallite sizes have been calculated to be in the range of 5–15 nm for the heat treatment powders. They are in agreement with the sizes determined from TEMs.

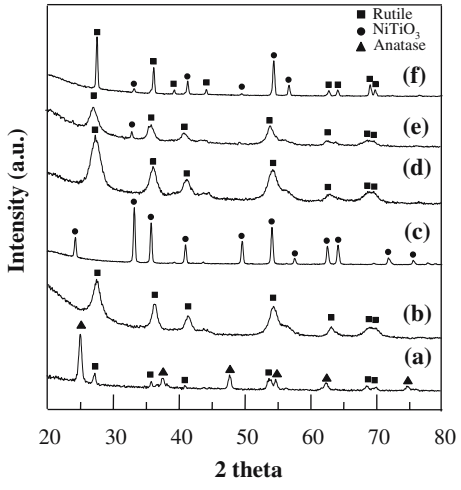

Figure 1. XRD patterns of powders (a) P-25 (b) rutile (c) $NiTiO_3$ (d) alloyed powder (e) alloyed powder after heat treatment (f) simple mixture powder (rutile + $NiTiO_3$).

The microstructure of the P-25, rutile, $NiTiO_3$, alloyed powder and novel nanocomposite powders were examined by TEM. The microstructures are shown in figure 2. In the case of P-25 powders, spherical particles were observed. In addition, the rutile particle had a chestnut bur shape with a size of 200–300 nm, in which the primary acicular particles are coagulated. The $NiTiO_3$ consisted of conglomerated spherical particles with a grain size of 50–100 nm. The alloyed powder consisted of spherical particles with an average grain size of less than 6 nm. Even though the novel nanocomposite TiO_2 powder had spherical particle, its SAD (selected Area electron Diffraction) pattern was slightly different from the alloyed powder. Except for the novel nanocomposite powder, all of the powders had a SAD pattern that was only one crystal structure. However, the novel nanocomposite TiO_2 powder consisted of nano-sized rutile TiO_2 and rhombohedral $NiTiO_3$. Also the particles were uniform with an average grain size less than 15 nm. The small grain size and uniforminity was caused by welding and fracture of the powder particle during ball milling. These results agree well with the XRD data in figure 1.

Figure 3 show the results of diffuse reflectance spectra result of P-25, rutile, $NiTiO_3$ powder, the alloyed powder, novel nanocomposite powder and simple mixture powder, respectively. From figure 4, it can be seen that the novel nanocomposite powder has the greatest wavelength shift and longest wavelength as compared

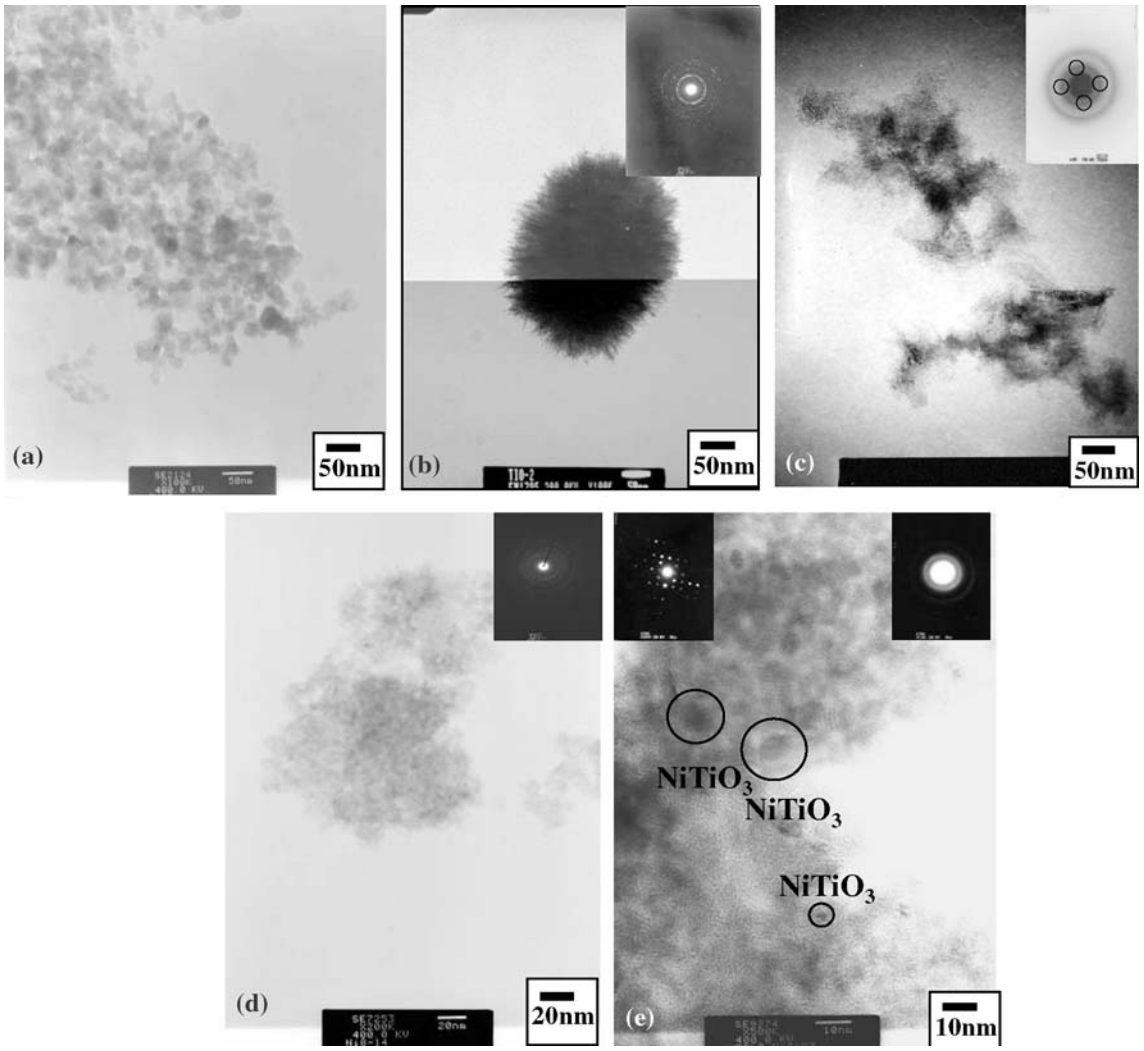

Figure 2. TEM micrographs of the powders (a) P-25 (b) rutile (c) $NiTiO_3$ (d) alloyed powder (e) alloyed powder after heat treatment.

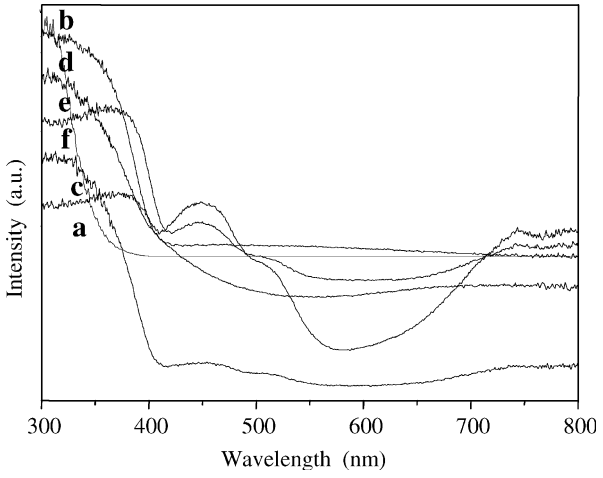

Figure 3. UV/VIS-DRS data (a) P-25 (b) rutile (c) $NiTiO_3$ (d) alloyed powder (e) alloyed powder after heat treatment (f) simple mixture powder (rutile + $NiTiO_3$).

with other powders. The most likely reason for the observed absorption shift might involve the $NiTiO_3$ produced by thermal treatment, which can form trapping $NiTiO_3$ band structure within the rutile band gap [16]. This trapping band structure detains the photoexited electrons and delay the recombination rate. So, the lifetime of the electron–hole pair is extended [17]. In contrast to the well-known rutile whose absorption edge is at about 410 nm, a novel nanocomposite TiO_2 exhibited obvious absorption in the visible light region over 650 nm. It indicates that even if the alloyed powder shifted the visible light region, the visible area was a little bit short and the novel nanocomposite powders (Ni-doped + $NiTiO_3$) have the ability to respond to visible light. The band gap was 1.84 eV which was estimated from the absorption edge of a novel nanocomposite TiO_2. This suggests that the novel nanocomposite TiO_2 has a greater ability to respond to the wavelength of the visible light region.

Figure 4 shows the photoluminescence spectra of the powders. The rutile and simple mixture powder had an

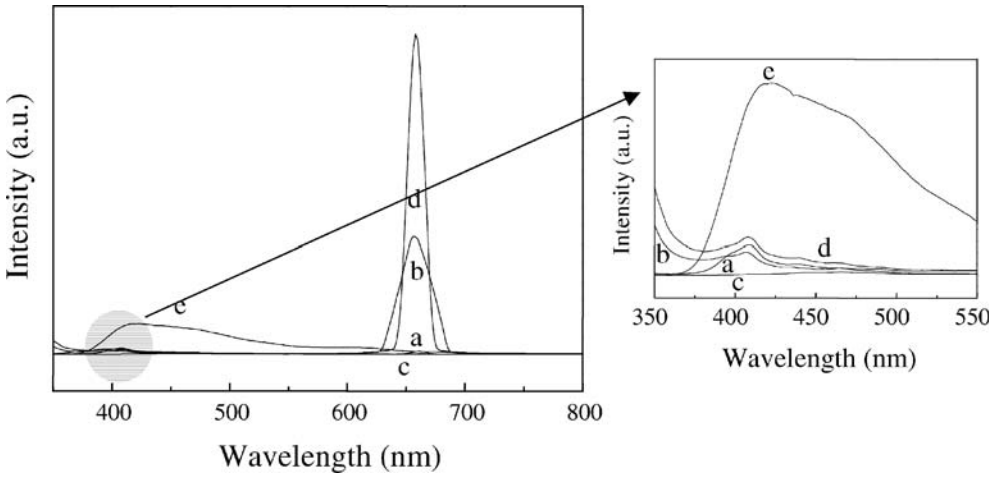

Figure 4. Photoluminescence data (a) rutile (b) $NiTiO_3$ (c) alloyed powder (d) alloyed powder after heat treatment (e) simple mixture powder (rutile + $NiTiO_3$).

emission peak at around 410 nm (3.02 eV) which corresponds to the rutile phase. And the alloyed powders showed that the emission peak shifted towards a longer wavelength region (454 nm = 2.72 eV) with decreasing peak intensity. It may be due to the fact that the new absorption was induced by localization of the trapping level in the TiO_2 band gap. This result agreed well with our previous experiment [18]. However, in the novel nanocomposite powder and the $NiTiO_3$ powder had intense emission peaks around 662 nm (1.87 eV). Also, the intensity of the novel nanocomposite powder was higher than the intensity of the $NiTiO_3$. This indicates that the $NiTiO_3$ reacted in the visible light region and the novel nanocomposite powder was strongly enhanced reaction ability in visible region as compared to $NiTiO_3$. Because the novel nanocomposite consisted of Ni-doped TiO_2 and $NiTiO_3$ was found that the lifetime of the electrons and holes were enhanced in comparison with rutile TiO_2, Ni-doped TiO_2 and single phase of $NiTiO_3$, as a result of electron or hole trapping at $NiTiO_3$ band gap [19].

Photocatalytic reaction of the TiO_2 powders under UV and visible light irradiation were evaluated by measuring the decomposition of 4-chloropenol, and the results are shown in figure 5. Under UV and visible light irradiation, the reaction ability of nanocomposite TiO_2 was much higher than that of P-25 and HPPLT rutile powders. And no degradation of 4-chlorolopenol was observed in the absence of TiO_2 powder or without irradiation. Under visible light irradiation, very small reaction of the P-25 was effect of fluorescence lamp (380–800 nm). It is very important that we synthesized a novel nanocomposite TiO_2 powder which shows phtocatalytic reaction under very long visible light range.

4. Conclusion

In summary, the novel photocatalyst powder of TiO_2 nanocomposite was synthesized by MA and heat treatment. The average grain size of the particle was less than 6 nm. The composite of Ni-doped TiO_2 and $NiTiO_3$ was formed by heat treatment and dramatically enhanced the ability in the visible light reaction. The UV/VIS DRS absorption showed that the novel nanocomposite TiO_2

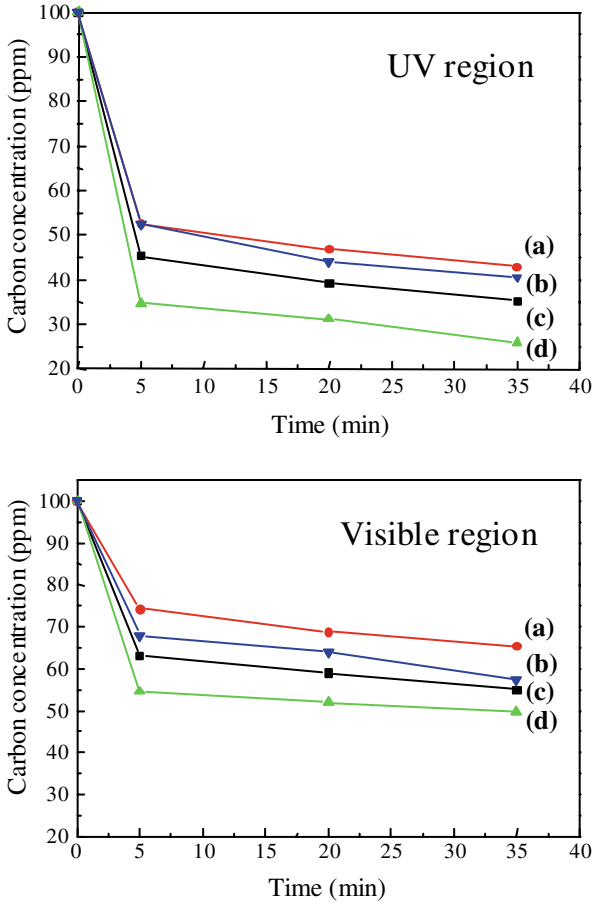

Figure 5. Photocatalytic decomposition of 4-Chrolophenol using various TiO_2 powders. (a) P-25 (b) $NiTiO_3$ (c) alloyed powder (d) alloyed powder after heat treatment.

had a higher wavelength rage (650–700 nm) than Ni-doped TiO_2 (480–500 nm) and the rutile powder (380–400 nm). PL spectrum of the novel nanocomposite TiO_2 showed a new emission peak toward the longer wavelength region, suggesting a decrease in the band gap (1.87 eV).

Acknowledgements

The present work is supported by the Energy Technology Academy Promotion.

References

[1] J.M. Kesselman, G.A. Shreve, M.R. Hoffmann and N.S. Lewis, J. Phys. Chem. 98 (1994) 13369.
[2] T. Morikawa, R. Asahi, T. Ohwaki, A. Aoki and Y. Taga, Jpn. T. Appl. Phys. 2(40) (2001) L561.
[3] X.Z. Li, F.B. Li, C.L. Yang and W.K. Ge, J. Photochem. Photobiol. A, Chem. 141 (2001) 209.
[4] T. Umebayashi, T. Yamaki, H. Itoh and K. Asai, Appl. Phy. Letters 81(3) (2002) 454.
[5] T. Ohno, M. Akiyoshi, T. Umebayashi, K. Asai, T. Mitsui and M. Matsumura, Appl. Catal. A: Gen. 265 (2004) 115.
[6] Y.J. Lin, Y.H. Chang and Y.S. Chang, Abs. 105, 204th Meeting, The Electrochemical Society, Inc.
[7] L. Zhou, S.Y. Zhang, J.C. Cheng, L.D. Zhang and Z. Zeng, Mat. Sci. Eng. B 49 (1997) 117.
[8] D.H. Kim, H.S. Park, S.J. Kim and K.S. Lee, Catal. Letters 100 (2005) 48.
[9] S.D. Park, Y.H. Cho, W.W. Kim and S.J. Kim, J. Solid State Chem. 146 (1999) 230.
[10] H.S. Kim, S.I. Hong and S.J. Kim, J. Mater. Process. Tech. 112 (2001) 109.
[11] B.D. Culity, *Elements of X-Ray Diffraction* 3 ed.(Addison-Wesley, Reading, MA, 2001) 170.
[12] R.A. Spurr and H. Myers, Anal. Chem. 29 (1957) 760.
[13] R.J. Brook, J. Am. Ceram. Soc., 52(1) (1969) 56.
[14] P.L. Chen and I.W. Chen, J. Am. Ceram. Soc. 79(7) (1996) 1793.
[15] D.H. Kim, H.S. Park, J.H. Jho, S.J. Kim and K.S. Lee, Mat. Sci. Eng. A (2005) in press.
[16] D.C. Cronemeryer, Phys. Rev. 113 (1959) 1222.
[17] K.Y. Jung and S.B. Park, Mater. Lett. 58 (2004) 2879.
[18] D.H. Kim, H.S. Hong, S.J. Kim and K.S. Lee, J. Alloy Compd. 375 (2004) 259.
[19] J. Moser, M. Gratzel and R. Gallay, Helv. Chim. Acta 70 (1987) 1596.